Photostability via a Sloped Conical Intersection: A CASSCF and RASSCF Study of Pyracylene

Martial Boggio-Pasqua, Michael A. Robb, and Michael J. Bearpark*

Chemistry Department, Imperial College London, South Kensington Campus, London SW7 2AZ, United Kingdom

Received: June 21, 2005; In Final Form: August 10, 2005

An extensive ab initio study of the ground- and excited-state potential energy surfaces of pyracylene is presented in this work. CASSCF calculations show that there is an accessible sloped S_0/S_1 conical intersection, which leads to ultrafast internal conversion and explains the observed photostability. RASSCF calculations (using a well-defined subset of the CASSCF configurations) are shown to be able to reproduce CASSCF results satisfactorily and will therefore be useful for larger systems where CASSCF is currently too expensive. MRCI and MRPT2 energy corrections are computed to assess the ionic character of the excited states. Finally, MMVB calculations are also benchmarked against CASSCF, to assess the reliability of this parametrized method for excited states of large conjugated polycyclic aromatic hydrocarbons.

Introduction

This study has three aims. The first is to present a consistent mechanism for the photophysics of pyracylene, a highly photostable polycyclic aromatic hydrocarbon,[1] based on critical points located on the ground-state and first three excited-state potential energy surfaces. The second aim is more general: to suggest a computational strategy to qualitatively study the excited states of large polyatomic conjugated systems, for which the number of electron configurations is beyond current computational resources for a full π-electron complete active space self-consistent field (CASSCF)[2] treatment. Finally, this work serves to benchmark the hybrid molecular mechanics−valence bond (MMVB)[3,4] method, whose original aim was to simulate CASSCF calculations for ground and excited states of conjugated hydrocarbons.[3]

Pyracylene is a polycyclic aromatic hydrocarbon (PAH) made up of two benzene (i.e., naphthalene) and two cyclopentene rings (see Chart 1). It was believed to be a major component of soot resulting from the incomplete combustion of acetylene or ethylene,[5] but Freiermuth et al.[1] discarded this suggestion in 1990. It was also proposed as a constituent of liquid fossil fuels, wood, or coal,[6,7] and even interstellar clouds.[8] Finally, the carbon framework of pyracylene is also the smallest elementary subunit that, when repeated, will generate the fullerenes such as C_{60} that are formed spontaneously by laser vaporization of graphite.[9] Thus, it has been employed as a model to study the interaction of transition metal complexes with fullerenes.[10]

The surprising physical properties of this remarkable hydrocarbon, in particular its very high photostability[1] and debatable aromaticity,[11,12] explain the numerous experimental and theoretical studies of this system. Trost and co-workers performed the first experimental work some 30 years ago.[13] They achieved the first synthesis of pyracylene and provided an extensive characterization of this compound.

At first, there was a conflict regarding the stability of pyracylene. On one hand, it was believed to be a very unstable antiaromatic molecule,[13] which was borne out by resonance energy calculations.[14] On the other hand, pyracylene was predicted to be the most stable hydrocarbon of composition $C_{14}H_8$ up to a temperature of 2500 K.[15] A major step forward was made 15 years ago when pyracylene was purified for the first time, and it was found that the reported instability was mainly due to the presence of some reactive impurities.[1] The same authors described pyracylene as "one of the most photostable organic chromophores we have had occasion to irradiate",[1] both as a solid and in solution. Fluorescence and intersystem crossing yields were below the limits of detection, and the authors attributed this remarkable photostability to the rapid radiationless deactivation of the excited states. We recently reported the existence of an S_0/S_1 conical intersection (CI) in pyracylene,[16] located using the MMVB method. The accessibility of this crossing was illustrated via dynamics simulations, and its topology (sloped in the classification introduced by Ruedenberg et al.)[17] accounts for the high photostability (see refs 17−22 for a discussion of the consequences of CI topology on excited-state lifetimes). However, there were some questions over whether the S_1 state obtained with MMVB is the state initially excited experimentally.

CHART 1: Pyracylene

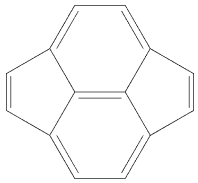

To our knowledge, this is the first ab initio study aiming to rationalize the mechanism behind the photostability of pyracylene. The reason is probably due to the huge computational effort currently required to access even qualitative information on the excited states of such a large system with ab initio methods. Nonetheless, MMVB has proved to be a very useful tool for generating initial nuclear configurations for CASSCF geometry optimizations,[23,24] and an extensive CASSCF study of pyracylene becomes feasible when using MMVB geometries as an initial guess. However, we are also concerned about

* Corresponding author. E-mail: m.bearpark@imperial.ac.uk.

10.1021/jp053354r CCC: $30.25
Published on Web 09/14/2005

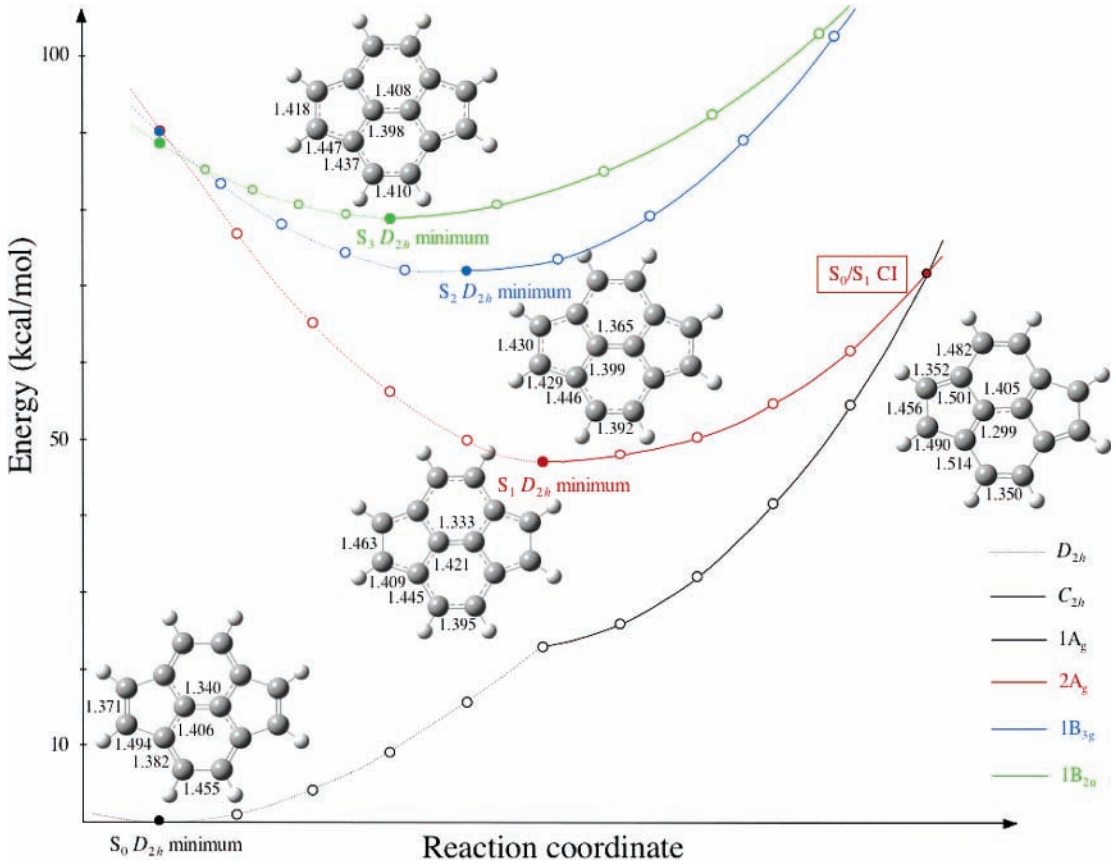

Figure 1. CASSCF potential energy profile for the electronic states involved in the photophysics of pyracylene. Filled circles correspond to optimized structures. Open circles correspond to interpolated structures. All bond lengths are in angstroms.

studying larger polycyclic aromatic hydrocarbons, which cannot currently be treated at the CASSCF level because the number of electronic configurations is too large. Therefore, we have tested a restricted active space self-consistent field (RASSCF)[25] approach to reduce the number of electron configurations for a given active space, and benchmarked these results against the CASSCF reference. This RASSCF approach should be useful for molecules where the full CASSCF calculations cannot be carried out.[26] Finally, this study also serves as a benchmark study for the MMVB method itself. Because of the computational resources required for CASSCF calculations, there is a lack of data for large polycyclic aromatic hydrocarbon systems to benchmark MMVB against. This is the first study to compare the MMVB potential against CASSCF for such a large active space (14e,14o). The largest to date was the study of the radical phenalenyl (13e,13o).[24]

The article is organized as follows: After a description of the computational methodology, we present the results of our extensive CASSCF calculations performed to explore the ground state and first three excited states of pyracylene. A full rationalization of the mechanism behind the high photostability of pyracylene is given. Next, we compare our RASSCF results against CASSCF and validate the method as a less expensive alternative to CASSCF. The effect of dynamic electron correlation (computed with MRCI/MRPT2) is also discussed. Finally, the MMVB potential is compared with CASSCF, and the successes and limitations of MMVB are emphasized.

Computational Details

The ground state (S_0) and first three excited electronic states (S_1-S_3) of pyracylene have been computed with CASSCF by distributing 14 π electrons in 14 π orbitals (14e,14o), generating around 6.9×10^5 electron configurations in D_{2h} symmetry and 1.38×10^6 in C_{2h}. The π-electronic states belong to the A_g, B_{3g}, B_{2u}, and B_{1u} irreducible representations of the D_{2h} point group. The basis set used was 4-31G,[27a] partly because this was the one used in the original parametrization of MMVB,[3] but also because it is flexible enough to describe valence states of small organic molecules.[27a] However, 6-31G*[27b,c] and Dunning's cc-pVTZ[28] were also used to assess basis set effects on the geometries with CASSCF, and to perform post-CASSCF correlated calculations (see below). Geometry optimizations were performed with D_{2h} and C_{2h} symmetry constraints using MMVB optimized structures as starting geometries. Energy single-point calculations were performed at linearly interpolated structures between the different critical structures (stationary points and CI).

We used the RASSCF approach to reduce the number of electron configurations by restricting the excitations in the wave function. This reduction is done by subdividing the active space into three categories: a set of orbitals with a limited number of vacancies (called the RAS1 space), a fully active orbital set (RAS2), and a set of orbitals with a limited number of electrons (RAS3). We limited the excitations from the RAS1 space to singles and doubles only, and allowed only two electrons at most in RAS3. The choice of the molecular orbitals making up the different restricted active spaces is critical. The idea is to include the most important orbitals (see below and Table S1 in the Supporting Information) for the electron correlation in the RAS2 space, as this is where no restriction in the excitations is imposed. Because the S_0/S_1 conical intersection is the most important critical structure (at which radiationless decay to the ground state takes place), and because the two states of interest have to be well described simultaneously in its vicinity to obtain

TABLE 1: CASSCF(14,14)/4-31G Energies for Pyracylene[a]

geometry	$\Delta E^{vert}(S_1-S_0)$	$\Delta E^{vert}(S_2-S_0)$	$\Delta E^{vert}(S_3-S_0)$	ΔE^{adiab}	$\Delta E(S_0)$	$\Delta E(S_1)$	$\Delta E(S_2)$	$\Delta E(S_3)$
S_0 minimum	90.5	90.3	88.9	0	0	43.2	18.6	9.7
S_1 minimum	24.4	51.7	63.1	47.3	22.9	0	2.9	6.8
S_2 minimum	34.9	54.4	63.5	71.7	17.3	4.9	0	1.6
S_3 minimum	48.0	60.9	66.0	79.2	13.1	13.8	2.3	0
S_0/S_1 CI	0.2	48.4	45.3		71.7	24.6	48.4	37.9

[a] All energies are in kcal/mol. $\Delta E^{vert}(S_n-S_0)$ values are the energy differences between state S_n and state S_0 at the geometry specified in the first column. ΔE^{adiab} values are the adiabatic (nonvertical) excitation energies. $\Delta E(S_n)$ values are the relative energies of state S_n at the geometry specified in the first column, with the S_n minimum energy as reference.

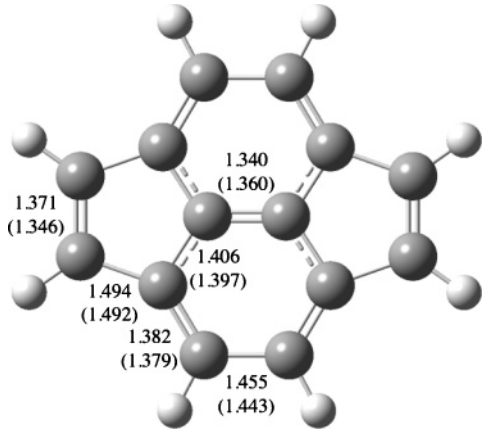

Figure 2. CASSCF(14,14)/4-31G optimized geometry for ground-state pyracylene. X-ray data are presented in parentheses. Distances are in angstroms.

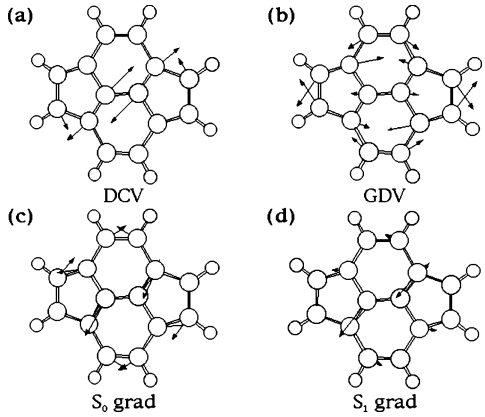

Figure 3. Branching space coordinates at S_0/S_1 CI: (a) derivative coupling vector (DCV); (b) gradient difference vector (GDV). Gradients at S_0/S_1 CI: (c) on S_0; (d) on S_1.

an accurate S_0-S_1 energy gap, we calibrated the RASSCF S_0-S_1 energy gap in the region of the crossing against the CASSCF value. We computed this energy gap at the optimized MMVB conical intersection geometry, where the degeneracy of the two states is lifted by 8.2 kcal/mol at the CASSCF level. We used all 14 π electrons in the RASSCF calculations, and the size of the RAS2 space was progressively increased until the S_0-S_1 energy gap became acceptable (typically error below 1 kcal/mol) at this geometry. The least expensive RASSCF calculation that was performed used two active orbitals in RAS2 (the highest occupied molecular orbital (HOMO) and lowest unoccupied molecular orbital (LUMO) necessary to describe the first two excited states at the ground-state geometry), for which the computed S_0-S_1 energy gap was 11.4 kcal/mol. We then enlarged RAS2 and shrank RAS1 and RAS3 so that the most occupied orbitals (orbitals with the largest occupation numbers) were left in RAS1 and the emptiest orbitals (orbitals with the lowest occupation numbers) were kept in RAS3. Using four active orbitals in RAS2, the S_0-S_1 energy gap is reduced to 7.0 kcal/mol. Using six orbitals in RAS2 brings the energy gap to 7.8 kcal/mol, just 0.4 kcal/mol from the target CASSCF value. The number of configurations is then around 48 000 (24 000 in D_{2h} symmetry), which makes the optimization of the S_0/S_1 crossing very cost-effective. This level of calculation, denoted RASSCF(14,4+6+4)[2,2], was then used to optimize the different electronic states of pyracylene with a comparison against CASSCF in mind. The optimized geometries we obtain are a further check of the active space partition used with RASSCF. Comparison with CASSCF orbital occupancies obtained for each excited state at other critical geometries (minima) was also made to ensure the partition is consistent for all of the geometries and pathways studied. It is important to note that conical intersection optimizations are very expensive calculations to run. State-averaged orbitals have to be used, and the orbital rotation derivative correction for using such orbitals becomes prohibitively expensive with such a large active space. However, this correction is usually small and therefore was neglected in the CASSCF conical intersection optimization. The correction on the gradient was included at the RASSCF level as it became affordable.

Dynamic correlation effects were estimated using two different approaches. The reason for doing this was to estimate the ionic character of the excited states, as the energies of ionic excited states are more sensitive to the treatment of dynamic electron correlation.[29] First, we applied the multireference configuration interaction (MRCI) method[30] using the RASSCF wave function as a reference and only allowing the active π electrons to be singly and doubly excited in the virtual orbital space. In this way, 14.7×10^6 electron configurations are generated and part of the valence−virtual correlation is recovered. (CASSCF was not used as a reference, as the resulting MRCI calculation would have generated too many configurations.) We will denote this approach π-MRCI as only π correlations are considered. π-MRCI calculations were performed at the D_{2h} critical points obtained at the RASSCF level. A similar strategy has been applied successfully to compute the vertical excitations of pyrene.[31] However, the dynamic polarization of the σ electrons resulting from simultaneous $\sigma\sigma^*$ and $\pi\pi^*$ excitations is omitted in π-MRCI. In practice it is currently impossible to include such correlation effects fully for molecules such as pyracylene and pyrene due to the computational bottlenecks inherent in the MRCI approach. Thus, in a second approach, the effect of the σ electrons was included through a perturbation treatment. We used the multireference second-order perturbation theory (MRPT2)[32] using the full CASSCF wave function as a reference, generating 48.7×10^6 electron configurations. MRPT2 calculations were performed at the D_{2h} geometries optimized at the CASSCF level, as this was the method used for computing the reference wave function. Similar approaches have been used to compute accurate electronic spectra of other large PAHs such as naphthalene,[33] phenanthrene,[34] anthracene,[35] and naphthacene.[35]

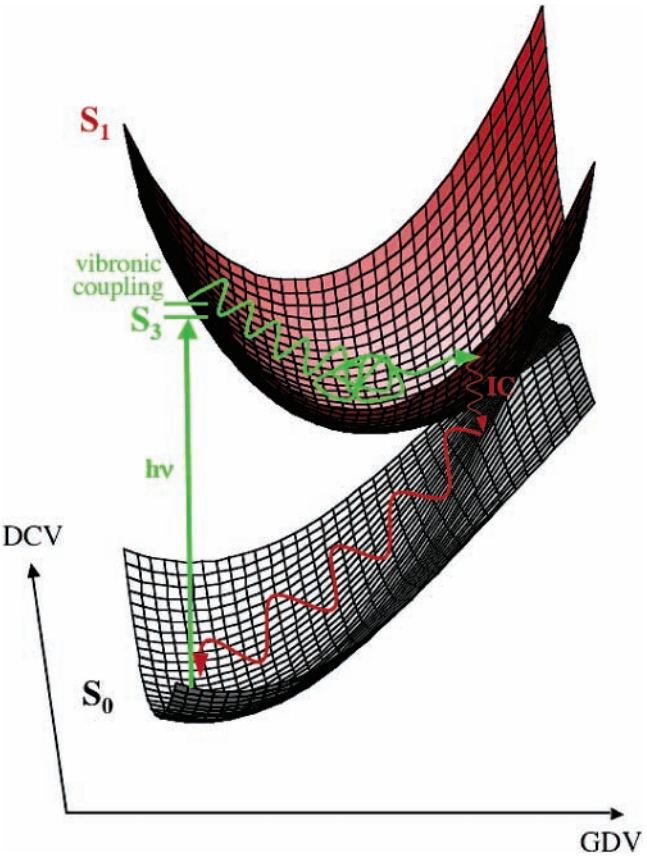

Figure 4. Schematic representation of the photophysical radiationless decay of pyracylene. DCV and GDV are the derivative coupling and gradient difference vectors, respectively.

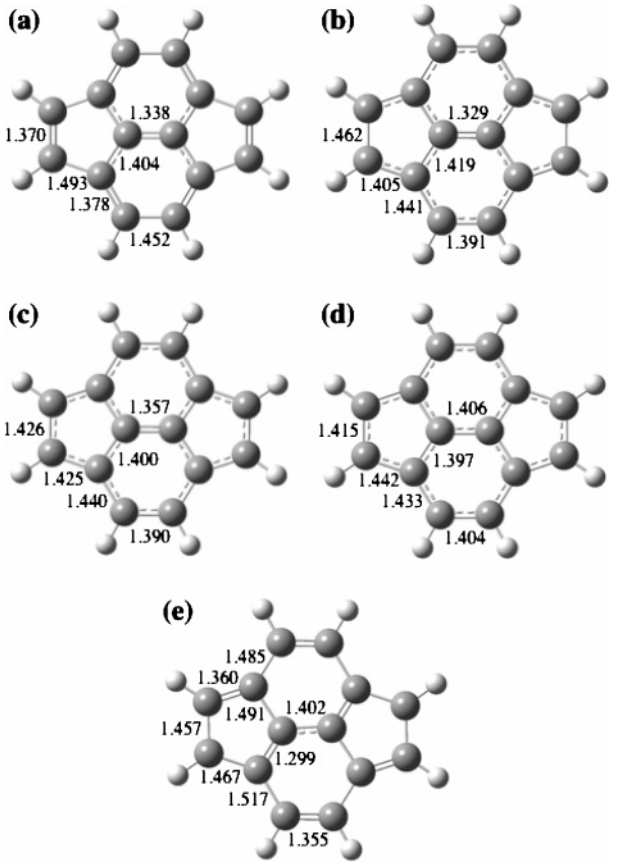

Figure 5. RASSCF(14,4+6+4)[2,2]/4-31G optimized structures of pyracylene: (a) S_0 D_{2h} minimum; (b) S_1 D_{2h} minimum; (c) S_2 D_{2h} minimum; (d) S_3 D_{2h} minimum; (e) S_0/S_1 C_{2h} conical intersection. All bond lengths are in angstroms.

Valence bond (VB) structures have been determined from the CASSCF wave functions by computing the spin-exchange density matrix P_{ij} in a localized orbital basis (see ref 36 for details). The elements of P_{ij} have a simple physical interpretation which is related to the spin coupling between the electrons localized in the orbitals residing on the atoms i and j.[37] An illustration of the meaning of these matrix elements can be found in ref 36. For example, the P_{ij} values for bonded and nonbonded atoms in an ideal VB function are 1.0 and −0.5, respectively, whereas a value of 0.5 indicates a resonating interaction. In this way, a direct comparison between CASSCF and MMVB is possible and identification of the electronic states can be made. The results of the MMVB calculations can be found in ref 16.

All calculations were performed with MOLPRO,[38] except for the P_{ij} calculations and the CASSCF conical intersection optimization, for which we used Gaussian.[39]

Results and Discussion

Photostability by Internal Conversion through a Sloped Conical Intersection. The results of our CASSCF calculations are summarized in Figure 1 and Table 1. Figure 1 displays the potential energy profile corresponding to the four electronic states involved in the photophysics of pyracylene along D_{2h} and C_{2h} distortion coordinates. These four states are the ground state $S_0(1\ ^1A_g)$ and the first three low-lying excited states $S_1(2\ ^1A_g)$, $S_2(1\ ^1B_{3g})$, and $S_3(1\ ^1B_{2u})$ (where the label S_n refers to the order obtained for 0−0 transitions, not vertically). Higher excited states were also computed, but they are well separated from the lower ones (see Table S2 for energy data on these higher excited states and Figure S1 for their structures). All four states S_0-S_3 have a D_{2h} minimum energy structure, and no lower C_{2h} minima could be located. The structures of the minima on each potential surface are also represented in Figure 1.

The CASSCF ground-state structure is shown in Figure 2 together with the X-ray structure of pyracylene.[1] Both structures are in good agreement, displaying D_{2h} symmetry with a pronounced alternation of bond lengths around the 12-π-electron periphery. The standard error is 0.015 Å with a maximum error of 0.025 Å for the double bonds in the cyclopentene rings. The CASSCF structure is also in good agreement with semi-empirical[1] and density functional theory[11,12] calculations, which all reproduce the pattern of single/double bond alternation observed experimentally.

The first excited state S_1 is covalent, and corresponds mainly to a doubly excited state resulting from the $(HOMO)^2 \rightarrow (LUMO)^2$ transition. On the other hand, the second excited state S_2 is a singly excited state with a strong ionic character originating from the HOMO → LUMO one-electron transition. The minimum energy structures of both states are similar to each other but quite different from the ground state S_0 (see Figure 1). The five central CC bond lengths are similar to the S_0 minimum, with the central double bond shorter in S_1 than it is in S_0, whereas it is longer in S_2. However, there is a complete inversion of the bond length alternation in the 12-π-electron periphery, with a somewhat more delocalized character (particularly in S_2). Finally, the S_3 state corresponds to a singly excited state (involving mainly a one-electron transition to the LUMO) and displays a minimum energy structure with a more delocalized π-electron system (smaller difference between longest and shortest bonds) compared to the first three states.

TABLE 2: RASSCF(14,4+6+4)[2,2]/4-31G Energies for Pyracylene[a]

geometry	$\Delta E^{vert}(S_1-S_0)$	$\Delta E^{vert}(S_2-S_0)$	$\Delta E^{vert}(S_3-S_0)$	ΔE^{adiab}	$\Delta E(S_0)$	$\Delta E(S_1)$	$\Delta E(S_2)$	$\Delta E(S_3)$
S_0 minimum	95.7	89.6	93.0	0	0	45.8	18.5	10.2
S_1 minimum	25.4	49.3	65.3	49.9	24.6	0	2.8	7.0
S_2 minimum	37.6	53.9	67.5	71.1	17.2	4.9	0	1.9
S_3 minimum	49.5	59.1	68.3	82.9	14.5	14.1	2.5	0
S_0/S_1 CI	0.2	45.9	45.0		68.3	18.5	43.0	30.5

[a] All energies are in kcal/mol. $\Delta E^{vert}(S_n-S_0)$ values are the energy differences between state S_n and state S_0 at the geometry specified in the first column. ΔE^{adiab} values are the adiabatic (nonvertical) excitation energies. $\Delta E(S_n)$ values are the relative energies of state S_n at the geometry specified in the first column, with the S_n minimum energy as reference.

TABLE 3: Excitation Energies in Pyracylene with Ab Initio Level[a]

	excitations					
	$S_0 \rightarrow S_1$		$S_0 \rightarrow S_2$		$S_0 \rightarrow S_3$	
ab initio level	vertical	adiabatic	vertical	adiabatic	vertical	adiabatic
CASSCF/4-31G	90.5	47.3	90.3	71.7	88.9	79.2
CASSCF/6-31G*	90.0	45.9	86.8	68.0	86.8	76.9
RASSCF/4-31G	95.7	49.9	89.6	71.1	93.0	82.9
RASSCF/6-31G*	94.9	48.1	85.8	67.2	90.0	80.0
π-MRCI/6-31G*	91.4	42.9	76.4	58.6	84.5	74.8
MRPT2/6-31G*	80.4	33.8	53.5	40.6	71.0	61.7
MRPT2/cc-pVTZ	77.2	31.2	47.1	35.3	66.8	58.7

[a] All energies are in kcal/mol. π-MRCI and MRPT2 calculations were performed at the RASSCF and CASSCF optimized geometries, respectively.

Along a C_{2h} distortion coordinate, a crossing between the S_0 and S_1 electronic states was located, forming a conical intersection (S_0/S_1 CI). An explanation for the existence of this structure is given in ref 16. The branching space of the two degeneracy-lifting coordinates is represented in Figure 3. The gradient difference vector (GDV) mainly involves a skeletal deformation of the periphery, whereas the derivative coupling vector (DCV) involves more vibrations from the internal CC bonds. Note that GDV corresponds mainly to the reaction coordinate. The most important feature of this conical intersection is that its topology is sloped.[40] Indeed, the crossing is higher in energy than the S_1 D_{2h} minimum, the gradients on the S_0 and S_1 surfaces at the crossing (see Figure 3c,d) are similar (parallel), and the forces (opposite the gradients) point toward the ground-state minimum.

CASSCF relative energies are collected in Table 1. The first three singlet excited states are very close in energy at the Franck−Condon geometry, lying around 90 kcal/mol above the ground state. In fact, the $S_3(1\ ^1B_{2u})$ state is the lowest, with S_1 and S_2 being quasi-degenerate. Both S_1 and S_2 are symmetry-forbidden, whereas the $S_3(1\ ^1B_{2u})$ state is optically active with a transition dipole moment equal to −0.495 au along the *y*-axis (axis in the molecular plane and bisecting the central CC bond). Because of the near degeneracy of these three states at this geometry, strong vibronic coupling will occur. Thus, population of the symmetry-forbidden states is expected as well. Moreover, because the S_3 state is the lowest state at the Franck−Condon geometry, it crosses the S_1 and S_2 states upon relaxation along a D_{2h} coordinate (Figure 1). These crossings occur in the region of the Franck−Condon geometry because the states are very close in energy. They provide efficient radiationless deactivation funnels for ultrafast internal conversion to the lowest S_1 minimum.

The adiabatic S_0-S_1 transition was measured at 650 nm (44 kcal/mol),[1] in good agreement with our CASSCF result (47.3 kcal/mol). The S_2 and S_3 minima are about 24 and 32 kcal/mol above S_1. Thus, S_1 is much more stabilized (43.2 kcal/mol) upon relaxation from the Franck−Condon region than S_2 and S_3 (18.6 and 9.7 kcal/mol, respectively). This can be explained by the complete inversion of the bond length alternation that S_1 has to undergo. However, while the S_1 state is strongly stabilized, the ground-state energy increases by 23 kcal/mol, resulting in a large decrease of the S_0/S_1 energy gap (to 24.4 kcal/mol) at the S_1 minimum. Finally, along a C_{2h} distortion, the two states eventually cross and the S_0/S_1 conical intersection lies about 20 kcal/mol above the S_1 minimum (14 kcal/mol with RASSCF/6-31G*), an energy well below the available energy in the system if vertically excited and therefore energetically accessible. Furthermore, because the crossing is sloped, the energies of the two states are close some way below the fully optimized crossing point. The energy barrier to the conical intersection may also be lowered at a higher level of calculation.

A simple mechanism emerges from Figure 1 accounting for the high photostability of pyracylene. The system is directly populated in the $1\ ^1B_{2u}$ electronic state, which is the lowest state at the Franck−Condon geometry and the only symmetry-allowed state. Nonetheless, the $2\ ^1A_g$ and $1\ ^1B_{3g}$ states are also initially populated via strong vibronic coupling with $1\ ^1B_{2u}$. Furthermore, the interstate crossings in the Franck−Condon region provide channels for ultrafast internal conversion to the S_1 and S_2 states. The S_1 state is probably the most favorable relaxation pathway as it is the most favorable route energetically (i.e., resulting in the largest energy stabilization). Population of S_2 would lead up eventually to internal conversion to S_1, as S_2 also crosses S_1 in the Franck−Condon region. After population of S_1, the system relaxes to the S_1 D_{2h} minimum where it can access a conical intersection because there is sufficient excess energy available and a well-defined coordinate belonging to the branching space of the crossing along a C_{2h} distortion coordinate. Internal conversion to the ground state can then efficiently take place. As the forces on S_0 point toward the S_0 minimum, there is only one relaxation pathway leading to the regeneration of the initial reactant. The mechanism is schematically depicted in Figure 4.

RASSCF: a Less Expensive Alternative for CASSCF Calculations. To reduce the computational effort required to solve the configuration interaction part of CASSCF, we used RASSCF to reduce the number of electron configurations while aiming to preserve the accuracy of the calculations. Thus, the target structures and energies are given by CASSCF. If

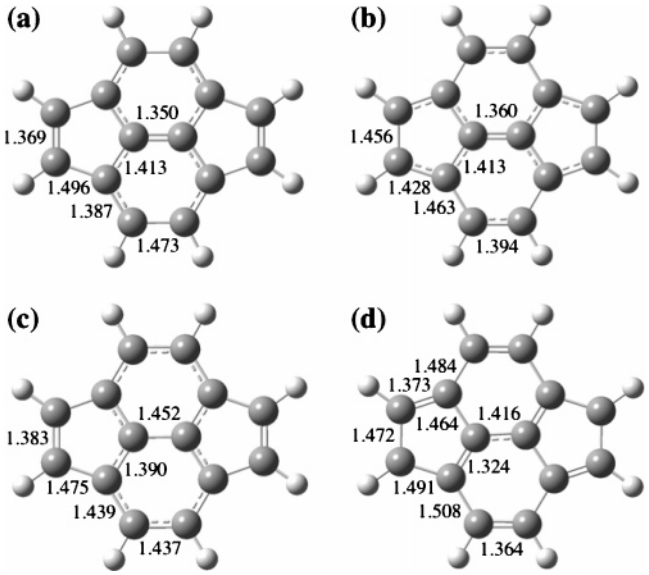

Figure 6. MMVB optimized structures from ref 16: (a) S_0 D_{2h} minimum; (b) S_1 D_{2h} minimum; (c) S_2 D_{2h} minimum; (d) S_0/S_1 C_{2h} CI.

successful, RASSCF could then be used in its own right for similar problems where CASSCF is computationally too demanding.

The RASSCF optimized structures are presented in Figure 5. Comparison with the CASSCF structures in Figure 1 shows the excellent agreement between the two methods: the standard error on the bond lengths of the minima does not exceed 0.005 Å with a maximum error of below 0.01 Å. The structure of the conical intersection is also well reproduced with a standard error in the bond lengths under 0.01 Å. The RASSCF branching space (presented in ref 16) is similar to the CASSCF result in Figure 3, and the topology of the CI is the same in both cases. However, with RASSCF we also found a slightly distorted S_1 minimum (Figure S2) with C_{2h} symmetry lying 1.2 kcal/mol below the D_{2h} minimum. Such a structure could not be located with CASSCF, and this weak localization of the bonds is probably due to the restricted number of electron configurations used. Nonetheless, this is a small perturbation in the topology of the S_1 surface.

RASSCF relative energies are collected in Table 2. Comparison with the CASSCF energetics presented in Table 1 attests to the good accuracy of the RASSCF calculations. The adiabatic excitation energies are well reproduced (in particular, the order of the electronic states is preserved), whereas the largest errors occur for the vertical excitation energies as the excited-state potential energy surfaces are steep in this region. Nonetheless, the three electronic excited states are still very close in energy (within 6.1 kcal/mol compared to 1.6 kcal/mol at CASSCF level).

Basis Set and Dynamic Correlation Effects. CASSCF and RASSCF geometry optimizations were also performed using the polarized 6-31G* basis set to assess the effect of enlarging the basis set. Table 3 collects the energy data, and Figure S3 displays the optimized structures. As expected, the basis set effect is small because these two methods only take into account the nondynamic (static) correlation (see ref 41 for a study of the convergence of the nondynamic and dynamic correlation energies of π electrons with basis set in planar hydrocarbons). Moreover, none of the geometries considered are highly distorted, so we do not expect polarization functions to much affect the structures at the CASSCF/RASSCF level. The

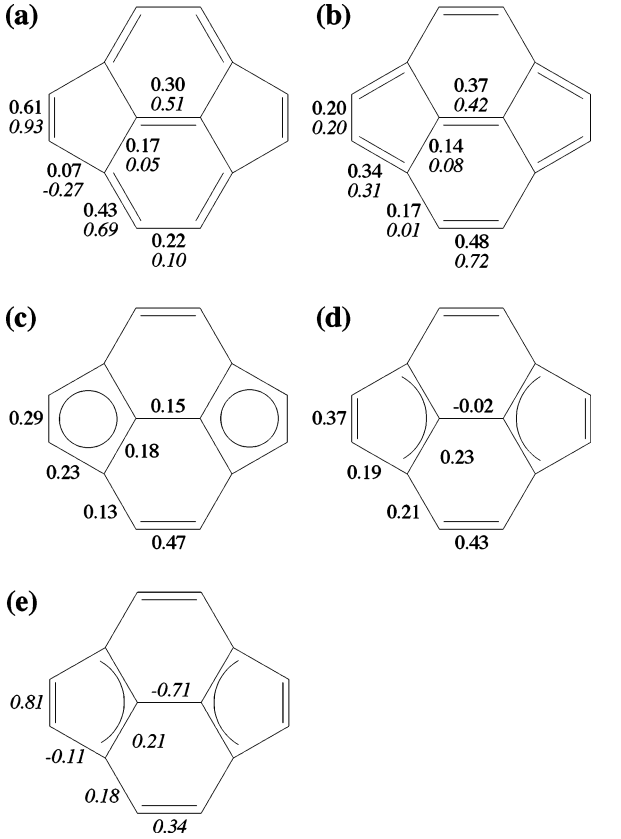

Figure 7. Valence bond structures obtained from spin-exchange density matrix calculations: (a) S_0 D_{2h} minimum; (b) S_1 D_{2h} minimum; (c) S_2 D_{2h} minimum; (d) S_3 D_{2h} minimum; (e) S_2 MMVB D_{2h} minimum. MMVB spin-exchange density matrix elements are in italics. CASSCF values are in normal print.

excitation energies match the ones computed with the 4-31G basis to within 4 kcal/mol. The bond lengths are identical to within 0.01 Å for the four D_{2h} minima. Note that the barrier to the conical intersection is lowered by 4.2 kcal/mol when using 6-31G* at the RASSCF level compared to RASSCF/4-31G.

We now discuss the effect of including dynamic electron correlation on the excited-state energies of pyracylene. We used π-MRCI to include the dynamic correlation resulting from the π electrons, which is known to be important in ionic states of conjugated systems.[42] MRPT2 was used to take into account the missing contribution to the dynamic correlation resulting from the σ electrons (dynamic polarization).

The MRCI excitation energies are very similar to the CASSCF ones for the S_1 and S_3 states, with changes less than 3 kcal/mol. However, π-MRCI brings the S_2 state down by about 10 kcal/mol further relative to the ground state. This is due to the strong ionic character of the S_2 state.

The MRPT2 excitation energies are much lower than the CASSCF and π-MRCI ones. Again, the effect is more pronounced for the S_2 state, whose adiabatic excitation energy is decreased by a further 18 kcal/mol from the π-MRCI value. This is due to the fact that the dynamic polarization effects on ionic states are particularly pronounced,[43] accounting for the stronger stabilization of the S_2 state at the MRPT2 level. Note that a better description of the dynamic correlation is attained when using the correlation consistent cc-pVTZ basis set, resulting in a further stabilization of the ionic state. However, it is important to note that the CASSCF/RASSCF results are qualitatively correct because the order of the electronic states stays the same.

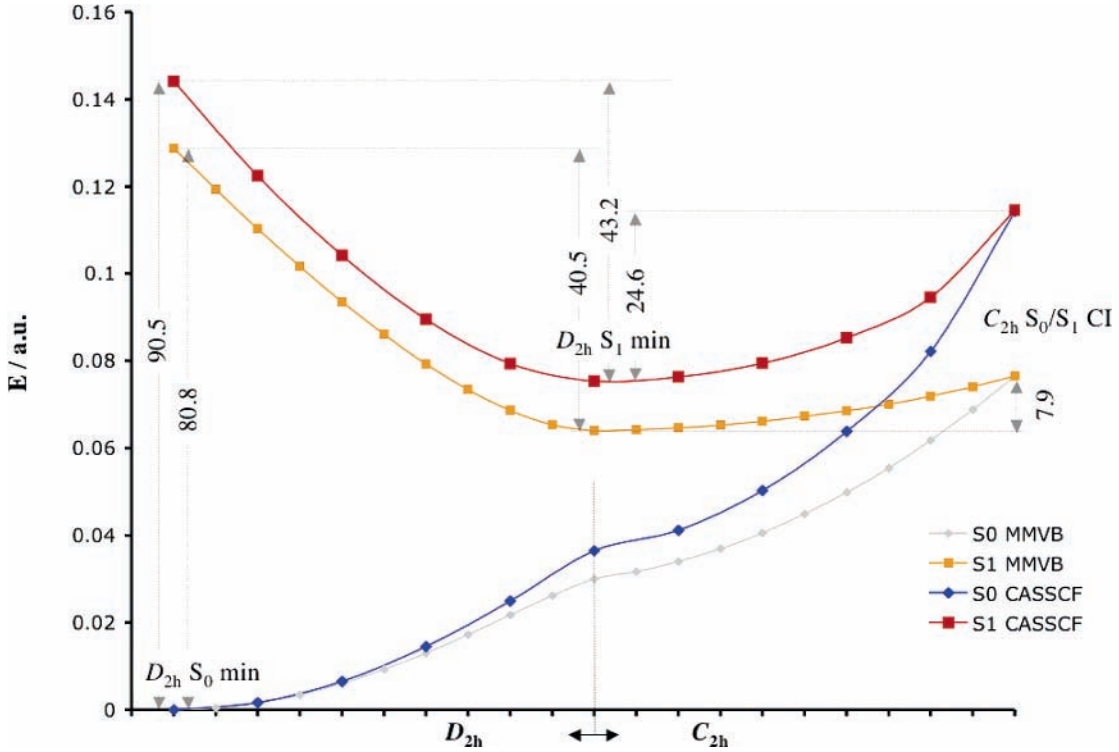

Figure 8. Comparison of MMVB and CASSCF potential energy profiles for S_0 and S_1 states of pyracylene. Relative energies are in kilocalories per mole.

Reliability of the Hybrid MMVB Method. The MMVB method is fully described in refs 16, 24, 44, and 45. It relies on a parametrized Heisenberg Hamiltonian coupled to a molecular mechanics force field, and for a particular choice of active space, the subset of electronic configurations with singly occupied localized orbitals is used. Thus, it cannot properly represent ionic states, which are dominated by charge-transfer terms, but it works well for covalent excited states.[46] Furthermore, MMVB can treat π systems with up to 30 active electrons at present, and is many orders of magnitude faster than CASSCF.[16]

The MMVB calculations of the S_0 and S_1 states of pyracylene are reported in ref 16. The optimized structures are collected in Figure 6. The S_0 and S_1 minima are in good qualitative agreement with CASSCF: the standard errors relative to the CASSCF geometries are 0.009 Å for the S_0 minimum (maximum error of 0.018 Å) and 0.016 Å for the S_1 minimum (maximum error of 0.027 Å). The conical intersection geometry is also well described (standard error of 0.018 Å) and provided a very good starting geometry for CASSCF/RASSCF geometry optimizations. However, the S_2 D_{2h} minimum found with MMVB does not correspond exactly to any structure optimized at the CASSCF level. This is the case even when comparing with CASSCF optimized minima for higher excited states ($S_4(1\ ^1B_{1u})$, $S_5(3\ ^1A_g)$). The S_2 MMVB structure most closely resembles the CASSCF S_3 minimum, although the central CC bond length differs by 0.044 Å.

VB structures have been determined from the CASSCF wave functions as explained in the Computational Details section. The comparison with the MMVB results is presented in Figure 7. This figure shows that the S_0 electronic structure is the same at the CASSCF and MMVB levels: for both methods, similar VB structures are generated. The S_1 state is also found to have the same nature with both CASSCF and MMVB. On the other hand, the CASSCF $S_2(1\ ^1B_{3g})$ VB structure does not match the MMVB S_2 result. This is mainly due to the fact that our current MMVB approach cannot properly describe ionic states because it includes only one active orbital/electron per atomic center, so with MMVB this state appears to be missing. However, the MMVB S_2 VB structure shows a spin coupling closer to the one for the CASSCF $S_3(1\ ^1B_{2u})$ state.

From an energy point of view, MMVB provides a qualitative description of the S_0 and S_1 potential energy surfaces, including the nonadiabatic reaction path from the S_0/S_1 CI. This is illustrated in Figure 8, which shows that the two potential energy profiles along the reaction path have the same shape. The main difference lies in the relative energy at the S_0/S_1 CI. The crossing occurs at 24.6 kcal/mol above the S_1 minimum at CASSCF/4-31G level instead of 7.9 kcal/mol with MMVB. Note that the crossing lies 14.3 kcal/mol above the S_1 minimum using RASSCF/6-31G*. CASSCF may well overestimate the barrier to the crossing, as in cyclohexadiene/hexatriene photochemical interconversion.[47]

Conclusion

The origin of the high photostability of pyracylene is described in this work. After photoexcitation, three low-lying excited states interacting through vibronic coupling are populated in the Franck−Condon region. The system quickly relaxes to the lowest S_1 excited state, where it can decay to the ground state through a sloped conical intersection. This internal conversion leads to the regeneration of pyracylene, as there is only one relaxation pathway in this region of the ground-state potential energy surface.

We found that RASSCF calculations were able to simulate CASSCF results with a good level of confidence. This approach can therefore be used to investigate potential energy surfaces of similar and possibly larger systems for which CASSCF is beyond present computational resources, provided that the RAS2 part of the active space is small.

Finally, MMVB is shown to be a useful method for determining structures and potential energy surfaces of polycyclic aromatic hydrocarbons. Although the descriptions of the

ground and first excited state potential energy surfaces of pyracylene are in good agreement with ab initio calculations, the higher excited states are not as well represented, which is probably due to a poor parametrization of MMVB for such states at present. However, in the CASSCF part of this study, we showed that the S_1 state responsible for radiationless decay to S_0 is the state well described by MMVB. This state is rapidly accessed in the vicinity of the vertically excited geometry. Using MMVB to describe the excited-state dynamics (as was done in ref 16) of this molecule is therefore realistic. Thus, we plan to use a similar approach to study the photoreactivity of larger conjugated systems. RASSCF, as a good approximation to CASSCF, will be used to determine the structures and potential energy surfaces of interest. Next, MMVB will be benchmarked against RASSCF to validate the MMVB potential surfaces of the state(s) responsible for radiationless decay. If the agreement is satisfactory, MMVB excited-state dynamics can be carried out.

Acknowledgment. This work has been supported by EPSRC UK (Grant GR/S94704/01). We thank the EPSRC National Service for Computational Chemistry Software (www.nsccs.ac.uk) for providing us the computing and software resources to perform the MOLPRO calculations on pyracylene.

Supporting Information Available: Cartesian coordinates for optimized CASSCF and RASSCF pyracylene structures. Table S1 explains the choice of orbitals in RASSCF, based on CASSCF orbital occupancies. Table S2 gives the energy data on several higher excited states of pyracylene, and Figure S1 displays the structures of these states. Figure S2 shows the slightly distorted C_{2h} minimum found with RASSCF on S_1. Figure S3 collects the pyracylene structures optimized with CASSCF and RASSCF using the 6-31G* basis set. Complete refs 38 and 39. This material is available free of charge via the Internet at http://pubs.acs.org.

References and Notes

(1) Freiermuth, B.; Gerber, S.; Riesen, A.; Wirz, J.; Zehnder, M. *J. Am. Chem. Soc.* **1990**, *112*, 738.

(2) Roos, B. O. *Adv. Chem. Phys.* **1987**, *69*, 399.

(3) Bernardi, F.; Olivucci, M.; Robb, M. A. *J. Am. Chem. Soc.* **1992**, *114*, 1606.

(4) Bearpark, M. J.; Robb, M. A.; Bernardi, F.; Olivucci, M. *Chem. Phys. Lett.* **1994**, *217*, 513.

(5) Crittenden, B. D.; Long, R. *Environ. Sci. Technol.* **1973**, *7*, 742.

(6) Schultz, J. L.; Kessler, T.; Friedel, R. A.; Sharkey, A. G. *Fuel* **1972**, *51*, 242.

(7) (a) Laflamme, R. E.; Hites, R. A. *Geochim. Cosmochim. Acta* **1978**, *42*, 289. (b) Lee, M. L.; Prado, G. P.; Howard, J. B.; Hites, R. A. *Biomed. Mass Spectrom.* **1977**, *4*, 182. (c) Howard, J. B.; Longwell, J. P. In *Polynuclear Aromatic Hydrocarbons: Formation, Metabolism, and Measurement*; Cooke, M., Dennis, A. J., Eds.; Battelle Press: Columbus, OH, 1983; p 27.

(8) Keller, R. In *Polycyclic Aromatic Hydrocarbons and Astrophysics*; Léger, A., et al., Eds.; Reidel: Dordrecht, The Netherlands, 1987; p 387.

(9) (a) Kroto, H. W.; Heath, J. R.; O'Brien, S. C.; Curl, R. F.; Smalley, R. E. *Nature* **1985**, *318*, 162. (b) Zhang, Q. L.; O'Brien, S. C.; Heath, J. R.; Liu, Y.; Curl, R. F.; Kroto, H. W.; Smalley, R. E. *J. Phys. Chem.* **1986**, *90*, 525. (c) Yang, S. H.; Pettiette, C. L.; Chesnovsky, O.; Smalley, R. E. *Chem. Phys. Lett.* **1987**, *139*, 233. (d) Heath, J. R.; Curl, R. F.; Smalley, R. E. *J. Chem. Phys.* **1987**, *87*, 4236. (e) Kroto, H. *Science* **1988**, *242*, 1139. (f) Aihara, J.; Hosoya, H. *Bull. Chem. Soc. Jpn.* **1988**, *61*, 2657. (g) Mallion, R. B. *Nature* **1987**, *325*, 760.

(10) Nunzi, F.; Sgamellotti, A.; Re, N. *J. Chem. Soc., Dalton Trans.* **2002**, *3*, 399 and references therein.

(11) Poater, J.; Solà, M.; Viglione, R. G.; Zanasi, R. *J. Org. Chem.* **2004**, *69*, 7537−7542, and references therein.

(12) Diogo, H. P.; Kiyobayashi, T.; Minas da Piedade, M. E.; Burlak, N.; Rogers, D. W.; McMasters, D.; Persy, G.; Wirz, J.; Liebman, J. F. *J. Am. Chem. Soc.* **2002**, *124*, 2065−2072.

(13) (a) Trost, B. M.; Bright, G. M. *J. Am. Chem. Soc.* **1967**, *89*, 4244. (b) Trost, B. M.; Nelsen, S. F.; Britelli, D. R. *Tetrahedron Lett.* **1967**, *40*, 3959. (c) Trost, B. M.; Bright, G. M. *J. Am. Chem. Soc.* **1968**, *90*, 2732. (d) Trost, B. M.; Bright, G. M. *J. Am. Chem. Soc.* **1969**, *91*, 3689. (e) Trost, B. M.; Bright, G. M.; Frihart, C.; Britelli, D. *J. Am. Chem. Soc.* **1971**, *93*, 737. (f) Trost, B. M. In *Topics in Nonbenzenoid Aromatic Chemistry*; Hirokawa Publishing Co.: Tokyo, 1973; Vol. I, p 243. (g) Trost, B. M.; Buhner, D.; Bright, G. M. *Tetrahedron Lett.* **1973**, *29*, 2787. (h) Trost, B. M.; Herdle, W. B. *J. Am. Chem. Soc.* **1976**, *98*, 4080.

(14) Aihara, J. *Bull. Chem. Soc. Jpn.* **1988**, *61*, 1451.

(15) Stein, S. E.; Fahr, A. *J. Phys. Chem.* **1985**, *89*, 3714.

(16) Bearpark, M. J.; Boggio-Pasqua, M.; Robb, M. A.; Ogliaro, F. Accepted for publication in *Theor. Chem. Acc.*

(17) Atchity, G. J.; Xantheas, S. S.; Ruedenberg, K. *J. Chem. Phys.* **1991**, *95*, 1862.

(18) Migani, A.; Olivucci, M. In *Conical Intersections: Electronic Stucture, Dynamics and Spectroscopy*; Domcke, W., Yarkony, D. R., Köppel, H., Eds.; Advanced Series in Physical Chemistry 15; World Scientific: Singapore, 2004; p 271.

(19) Paterson, M. J.; Robb, M. A.; Blancafort, L.; DeBellis, A. D. *J. Am. Chem. Soc.* **2004**, *126*, 2912.

(20) De Vico, L.; Page, C. S.; Garavelli, M.; Bernardi, F.; Basosi, R.; Olivucci, M. *J. Am. Chem. Soc.* **2002**, *124*, 4124.

(21) Ben-Nun, M.; Molnar, F.; Schulten, K.; Martínez, T. J. *Proc. Natl. Acad. Sci.* **2002**, *99*, 1769.

(22) Yarkony, D. R. *J. Chem. Phys.* **2001**, *114*, 2601.

(23) (a) Bearpark, M. J.; Bernardi, F.; Clifford, S.; Olivucci, M.; Robb, M. A.; Smith, B. R.; Vreven, T. *J. Am. Chem. Soc.* **1996**, *118*, 169. (b) Bearpark, M. J.; Celani, P.; Jolibois, F.; Olivucci, M.; Robb, M. A.; Bernardi, F. *Mol. Phys.* **1999**, *96*, 645. (c) Boggio-Pasqua, M.; Ravaglia, M.; Bearpark, M. J.; Garavelli, M.; Robb, M. A. *J. Phys. Chem. A* **2003**, *107*, 11139.

(24) Bearpark, M. J.; Boggio-Pasqua, M. *Theor. Chem. Acc.* **2003**, *110*, 105.

(25) (a) Olsen, J.; Roos, B. O.; Jørgensen, P.; Jensen, H. J. A. *J. Chem. Phys.* **1988**, *89*, 2185. (b) Malmqvist, P. A.; Rendell, A.; Roos, B. O. *J. Phys. Chem.* **1990**, *94*, 5477.

(26) This contrasts with our use of RASSCF to extend a CASSCF active space and recover dynamic correlation for ionic states (see ref 29). However, both contrasting approaches rely on using RASSCF with a small subset of the full CASSCF configuration list for a particular orbital active space.

(27) (a) Ditchfield, R.; Herhe, W. J.; Pople, J. A. *J. Chem. Phys.* **1971**, *54*, 724. (b) Herhe, W. J.; Ditchfield, R.; Pople, J. A. *J. Chem. Phys.* **1972**, *56*, 2257. (c) Harihan, P. C.; Pople, J. A. *Theor. Chim. Acta* **1973**, *28*, 213.

(28) Dunning, T. H. *J. Chem. Phys.* **1989**, *90*, 1007.

(29) Boggio-Pasqua, M.; Bearpark, M. J.; Klene, M.; Robb, M. A. *J. Chem. Phys.* **2004**, *120*, 7849.

(30) (a) Werner, H.-J.; Knowles, P. J. *J. Chem. Phys.* **1988**, *89*, 5803. (b) Knowles, P. J.; Werner, H.-J. *Chem. Phys. Lett.* **1988**, *145*, 514.

(31) Bito, Y.; Shida, N.; Toru, T. *Chem. Phys. Lett.* **2000**, *328*, 310.

(32) Celani, P.; Werner, H.-J. *J. Chem. Phys.* **2000**, *112*, 5546.

(33) (a) Hashimoto, T.; Nakano, H.; Hirao, K. *J. Chem. Phys.* **1996**, *104*, 6244. (b) Rubio, M.; Merchán, M.; Ortí, E.; Roos, B. O. *Chem. Phys.* **1994**, *179*, 395.

(34) González-Luque, R.; Serrano-Andrés, L.; Merchán, M.; Fülscher, M. P. *Theor. Chem. Acc.* **2003**, *110*, 224.

(35) Kawashima, Y.; Hashimoto, T.; Nakano, H.; Hirao, K. *Theor. Chem. Acc.* **1999**, *102*, 49.

(36) Blancafort, L.; Celani, P.; Bearpark, M. J.; Robb, M. A. *Theor. Chem. Acc.* **2003**, *110*, 92.

(37) McWeeny, R.; Sutcliffe, B. T. In *Molecular Quantum Mechanics*; Academic Press: New York, 1969; pp 148−170.

(38) Werner, H.-J.; et al. *MOLPRO*, version 2002.6; Birmingham, UK, 2003.

(39) Frisch, M. J.; et al. *Gaussian Development Version*, revision B.07; Gaussian, Inc.: Pittsburgh, PA, 2003.

(40) Atchity, G. J.; Xantheas, S. S.; Ruedenberg, K. *J. Chem. Phys.* **1991**, *95*, 1862−1876.

(41) Maksic, Z. B.; Baric, D.; Petanjek, I. *J. Phys. Chem. A* **2000**, *104*, 10873−10881.

(42) Cave, R. J. In *Modern Electronic Structure Theory And Applications In Organic Chemistry*; Davidson, E. R.; Ed.; World: Singapore, 1997; p 239.

(43) (a) Serrano-Andrés, L.; Merchán, M.; Nebot-Gil, I.; Lindh, R.; Roos, B. O. *J. Chem. Phys.* **1993**, *98*, 3151. (b) Cave, R. J.; Davidson, E. R. *J. Chem. Phys.* **1988**, *92*, 614. (c) Cave, R. J.; Davidson, E. R. *Chem. Phys. Lett.* **1988**, *148*, 190.

(44) Bernardi, F.; Olivucci, M.; Robb, M. A. *J. Am. Chem. Soc.* **1992**, *114*, 1606.

(45) Bearpark, M. J.; Robb, M. A.; Bernardi, F.; Olivucci, M. *Chem. Phys. Lett.* **1994**, *217*, 513.

(46) Bearpark, M. J.; Bernardi, F.; Olivucci, M.; Robb, M. A. *J. Phys. Chem. A* **1997**, *101*, 8395.

(47) Celani, P.; Ottani, S.; Olivucci, M.; Bernardi, F.; Robb, M. A. *J. Am. Chem. Soc.* **1994**, *116*, 10141.